

Interface properties in three-component Bose-Einstein condensates

Keisuke Jimbo¹ and Hiroki Saito¹

¹*Department of Engineering Science, University of Electro-Communications, Tokyo 182-8585, Japan*
(Dated: November 15, 2021)

Interface properties of a three-component Bose-Einstein condensate, in which component 3 is sandwiched by components 1 and 2 at the interface, are investigated. It is shown that component 3 can serve as a surfactant: the net interfacial tension is reduced by the presence of component 3. We calculate the interfacial tension as a function of the interaction coefficients. The stability of the interface is studied by Bogoliubov analysis. When the interfacial tension has a spatial gradient, interfacial flow is induced, which resembles the Marangoni flow.

I. INTRODUCTION

Surfactants lower the interfacial tension between two immiscible fluids. For example, soap molecules enter the interface between oil and water, lowering the interfacial tension. The interfacial tension is decreased because soap molecules have an affinity for both oil and water, which changes the interface structure. In this paper, we consider an analogous situation at the interface in three-component Bose-Einstein condensates (BECs), in which two immiscible components form an interface and the third component enters that interface.

Multicomponent BECs have been studied extensively both experimentally and theoretically. Two-component BECs were realized by using atoms in different hyperfine states [1] and different atomic species [2]. Miscibility of a two-component BEC depends on the inter- and intra-component interactions, which can be controlled by the Feshbach resonance technique [3, 4]. When the two components are immiscible, phase separation occurs and interfaces are formed [5–8]. The static and dynamic properties of such interfaces have been investigated theoretically [9–21]. The interfacial tension coefficients for an immiscible two-component BEC were obtained analytically and numerically in Refs. [12, 15, 16]. Dynamical instabilities [22–33], such as Rayleigh-Taylor and Kelvin-Helmholtz instabilities, were shown to deform the interface between two superfluids, as in the case of classical fluids. However, all the above studies focus on two-component interfaces; the interface of a three-component BEC has hitherto not been explored [34].

Let us suppose components 1 and 2 have segregated to either side of the interface, and a small amount of component 3 is localized at the interface (see Fig. 1). We will also assume that the repulsive interaction between components 1 and 2 is strong, while those between components 1 and 3 and between components 2 and 3 are moderate. In the absence of component 3, components 1 and 2 are in direct contact at the interface, in which case the interfacial tension becomes large owing to the strong repulsion [12, 15, 16]. On the other hand, if there is a component 3 lying between components 1 and 2, so that components 1 and 2 have no direct contact, the interfacial tension is suppressed because of the moderate repulsion between components 1 and 3 and between components 2

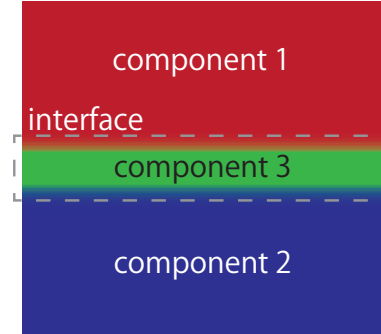


FIG. 1. Schematic of a three-component interface, in which component 3 is sandwiched by components 1 and 2. The whole region inside the dashed square is regarded as the three-component interface.

and 3. Thus, the interfacial tension is decreased by the presence of component 3 at the interface: component 3 can be regarded as a surfactant.

In this paper, we will show numerically and variationally that the above prediction is true and that the third component can play the role of surfactant at the interface. The interfacial tension is calculated for various parameters. We also perform Bogoliubov analysis to examine the stability of the three-component interface. The latter part of this paper investigates the dynamics of the system with a spatial gradient in interfacial tension. We will show that a mass current is induced near the interface such that the gradient in interfacial tension is compensated, similarly to Marangoni flow [42] in classical fluids.

The remainder of the paper is organized as follows. Section II focuses on the static properties of the three-component interface, including calculations of the interfacial tension, variational analysis, and Bogoliubov analysis. Section III numerically investigates the dynamics of Marangoni flow. Section IV presents the conclusions of this study.

II. STATIC PROPERTIES

A. Interfacial tension

We consider a three-component BEC of dilute gases in a uniform space at zero temperature. In the mean-field approximation, the energy of the system is given by

$$E = \int d\mathbf{r} \left[\sum_{j=1}^3 \left(-\psi_j^* \frac{\hbar^2}{2m_j} \nabla^2 \psi_j + \frac{g_{jj}}{2} |\psi_j|^4 \right) + \sum_{j < j'} g_{jj'} |\psi_j|^2 |\psi_{j'}|^2 \right], \quad (1)$$

where $\psi_j(\mathbf{r})$ is the macroscopic wave function and m_j is the atomic mass of component j ($j = 1, 2, \text{ and } 3$). The interaction coefficients in Eq. (1) are defined as $g_{jj'} = 2\pi\hbar^2 a_{jj'}/m_{jj'}$, where $a_{jj'}$ is the s -wave scattering length and $m_{jj'}$ is the reduced mass between components j and j' . We treat the problem in the grand canonical ensemble, and the grand potential,

$$\Omega = E - \sum_{j=1}^3 \mu_j N_j, \quad (2)$$

is minimized in the equilibrium state, where μ_j is the chemical potential and

$$N_j = \int d\mathbf{r} |\psi_j(\mathbf{r})|^2 \quad (3)$$

is the number of atoms in component j . The macroscopic wave functions $\psi_j(\mathbf{r})$ in the equilibrium state thus obey $\delta\Omega/\delta\psi^*(\mathbf{r}) = 0$, which gives the coupled Gross-Pitaevskii (GP) equations,

$$-\frac{\hbar^2}{2m_j} \nabla^2 \psi_j + \sum_{j'=1}^3 g_{jj'} |\psi_{j'}|^2 \psi_j = \mu_j \psi_j. \quad (4)$$

The miscibility of multicomponent BECs is determined by the interaction coefficients $g_{jj'}$. The uniformly mixed state of components j and j' is unstable against phase separation, when the inequality

$$g_{jj'}^2 > g_{jj} g_{j'j'} \quad (5)$$

is satisfied [38]. This immiscibility condition can also be extended to the three-component BEC [39]: the three components are immiscible with each other, when all pairs of components satisfy Eq. (5), that is,

$$g_{12}^2 > g_{11} g_{22} \quad g_{13}^2 > g_{11} g_{33}, \quad g_{23}^2 > g_{22} g_{33}. \quad (6)$$

In this paper, we assume that the interaction coefficients satisfy this immiscibility condition for a three-component BEC.

We consider a situation in which components 1 and 2 have uniform densities $n_{1\infty}$ and $n_{2\infty}$ at $z = -\infty$ and

$z = \infty$, respectively, and the interface between them is located at $z = 0$, around which component 3 is localized. The system is assumed to be uniform in the x and y directions and the GP equation (4) reduces to

$$-\frac{\hbar^2}{2m_j} \psi_j''(z) + \sum_{j'=1}^3 g_{jj'} |\psi_{j'}(z)|^2 \psi_j(z) = \mu_j \psi_j(z) \quad (7)$$

with $\mu_1 = g_{11} n_{1\infty}$ and $\mu_2 = g_{22} n_{2\infty}$, where the boundary conditions are $\psi_1(z = -\infty) = \sqrt{n_{1\infty}}$ and $\psi_2(z = \infty) = \sqrt{n_{2\infty}}$. The pressures on either side of the interface must be balanced with each other as

$$\frac{g_{11} n_{1\infty}^2}{2} = \frac{g_{22} n_{2\infty}^2}{2} \equiv P. \quad (8)$$

Multiplying Eq. (7) by $\psi_j'(z)$ and integrating the sum of the three equations with respect to z , we obtain

$$\sum_{j=1}^3 \left[-\frac{\hbar^2}{2m_j} (\psi_j')^2 + \frac{g_{jj}}{2} \psi_j^4 - \mu_j \psi_j^2 \right] + \sum_{j>j'} g_{jj'} \psi_j \psi_{j'} + C = 0, \quad (9)$$

where C is an integration constant and $\psi_j(z)$ is taken to be real without loss of generality. In the limit $z \rightarrow \pm\infty$, the first summation in Eq. (9) becomes $-P$ and the second summation vanishes; therefore, the constant C must be P . Substitution of Eq. (9) into Eq. (2) gives

$$\Omega = -PV + 2 \int d\mathbf{r} \sum_{j=1}^3 \frac{\hbar^2}{2m_j} (\psi_j')^2, \quad (10)$$

where V is the volume of the system. Since $\psi_j'(z)$ is nonzero only near the interface and vanishes elsewhere, the second term on the right-hand side of Eq. (10) arises only from the interface region. Thus, the interfacial tension σ can be expressed as

$$\sigma = 2 \int_{-\infty}^{\infty} dz \sum_{j=1}^3 \frac{\hbar^2}{2m_j} (\psi_j')^2. \quad (11)$$

This expression is similar to the one derived for two-component systems [16].

We numerically solve the GP equation (7) to obtain the equilibrium state $\psi_j(z)$, and using this, we calculate the interfacial tension of the three-component interface by Eq. (11). In order to reduce the number of parameters, we assume $m_1 = m_2 = m_3 \equiv m$ and $g_{11} = g_{22} = g_{33} \equiv g$ in the following calculations. We also assume $\mu_1 = \mu_2$, and hence $n_{1\infty} = n_{2\infty} \equiv n_\infty$. We normalize length, time, energy, and density by $\xi = \hbar/(2mgn_\infty)^{1/2}$, $\hbar/(gn_\infty)$, gn_∞ , and n_∞ , respectively. In this unit, $g_{11} = g_{22} = g_{33} = 1$ and $\mu_1 = \mu_2 = 1$. The variable parameters are thus g_{12} , g_{13} , g_{23} , and μ_3 . To obtain the solution for Eq. (7), we solve the imaginary-time GP equation as

$$\frac{\partial \psi_j}{\partial \tau} = \frac{1}{2} \psi_j'' - \sum_{j'=1}^3 g_{jj'} |\psi_{j'}|^2 \psi_j + \mu_j \psi_j, \quad (12)$$

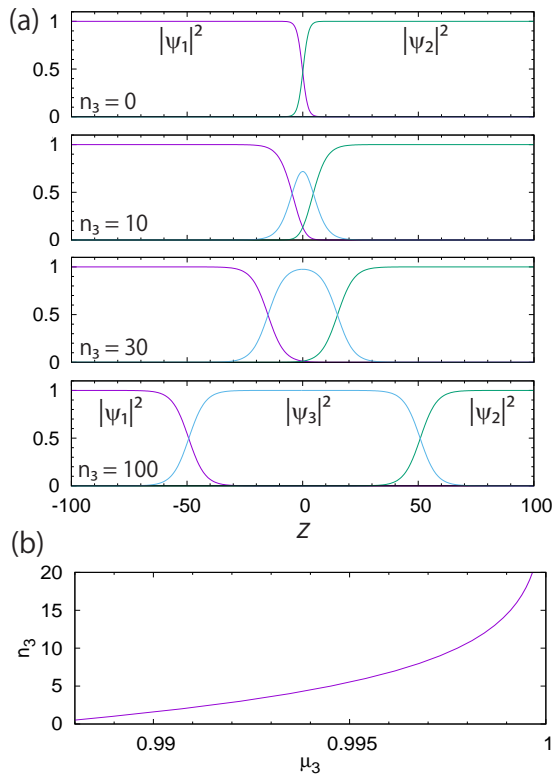


FIG. 2. Flat-interface equilibrium states. (a) Density profile of each component near the interface for $n_3 = 0, 10, 30$, and 100. (b) Areal density n_3 as a function of the chemical potential μ_3 for component 3. The parameters are $g_{12} = 1.1$ and $g_{13} = g_{23} = 1.01$.

using the pseudospectral method [40]. The initial state of the imaginary-time evolution is taken to be an appropriate state, e.g., $\psi_1(z) = \theta(-z)$, $\psi_2(z) = \theta(z)$, and $\psi_3(z) = \exp(-z^2)$, so that it converges to the desired interface state for large imaginary times, where $\theta(z)$ is the Heaviside step function. We take a large enough space so that the boundary does not affect the interface region.

Figure 2(a) shows the density profile $|\psi_j(z)|^2$ around the interface for different values of μ_3 . The intercomponent interaction coefficients are taken to be $g_{12} = 1.1$ and $g_{13} = g_{23} = 1.01$, which satisfy the immiscibility condition in Eq. (6). For $\mu_3 = 0$, component 3 vanishes, and a two-component (1 and 2) interface is realized, as shown in the uppermost panel in Fig. 2(a). The number of atoms n_3 in component 3 per unit area of the interface is given by

$$n_3 = \int |\psi_3(z)|^2 dz, \quad (13)$$

which is a monotonically increasing function of μ_3 , as shown in Fig. 2(b). (Note that the numerical values of n_3 are normalized by $n_\infty \xi$ in the present unit of normalization.) As n_3 increases, component 3 localized near the interface pushes away components 1 and 2, and components 1 and 2 are detached from each other ($n_3 = 30$

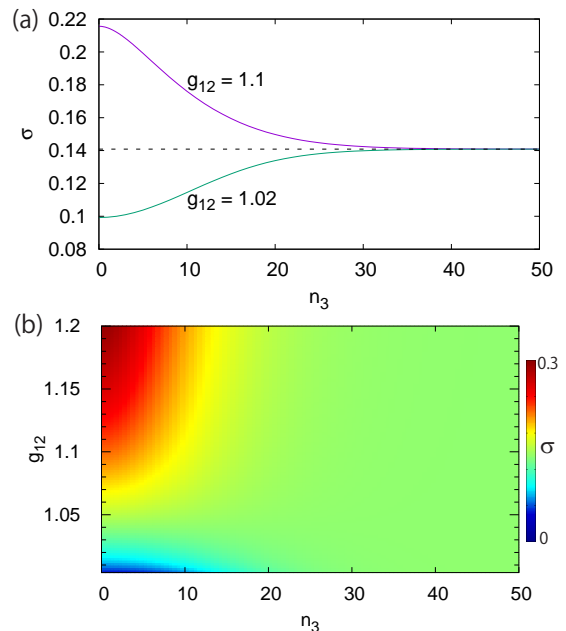


FIG. 3. Interfacial tension σ for $g_{13} = g_{23} = 1.01$. (a) n_3 dependence for $g_{12} = 1.1$ and $g_{12} = 1.02$. The horizontal dashed line represents $\sigma_{\text{binary}}(g_{13}) + \sigma_{\text{binary}}(g_{23}) \simeq 0.14$. (b) Dependence of σ on g_{12} and n_3 .

in Fig. 2(a)). When n_3 increases further ($n_3 = 100$ in Fig. 2(a)), component 3 becomes a plateau, which separates the two distinct (1-3 and 2-3) interfaces. In this paper, such a structure, as a whole, is also regarded as a single three-component interface.

We calculate the interfacial tension σ using Eq. (11) for the equilibrium state. Figure 3(a) shows σ as a function of n_3 . The case of $g_{12} = 1.1$ corresponds to the condition in Fig. 2. In this case, the interfacial tension σ decreases with increasing n_3 . Since the interfacial tension is decreased by the presence of component 3, we can say that component 3 plays the role of surfactant. By contrast, for $g_{12} = 1.02$, σ increases with n_3 . Figure 3(b) shows the dependence of σ on g_{12} and n_3 . The critical value of g_{12} for the surfactant behavior is $g_{12} \simeq 1.04$, above which σ is a decreasing function of n_3 .

We denote the interfacial tension of the two-component interface by $\sigma_{\text{binary}}(g_{\text{inter}})$, as a function of the intercomponent interaction coefficient g_{inter} (the intracomponent interaction coefficients being normalized to unity). When g_{inter} satisfies $g_{\text{inter}} - 1 \ll 1$, an approximate expression for the interfacial tension σ_{binary} of a two-component BEC can be derived as [12, 15, 16] (in the present unit of normalization)

$$\sigma_{\text{binary}}(g_{\text{inter}}) \simeq \sqrt{\frac{g_{\text{inter}} - 1}{2}}. \quad (14)$$

In Fig. 3(a), the interfacial tension at $n_3 = 0$ is $\sigma \simeq 0.216$ for $g_{12} = 1.1$ and $\sigma \simeq 0.099$ for $g_{12} = 1.02$, namely, $\sigma_{\text{binary}}(1.1) \simeq 0.216$ and $\sigma_{\text{binary}}(1.02) \simeq 0.099$. These

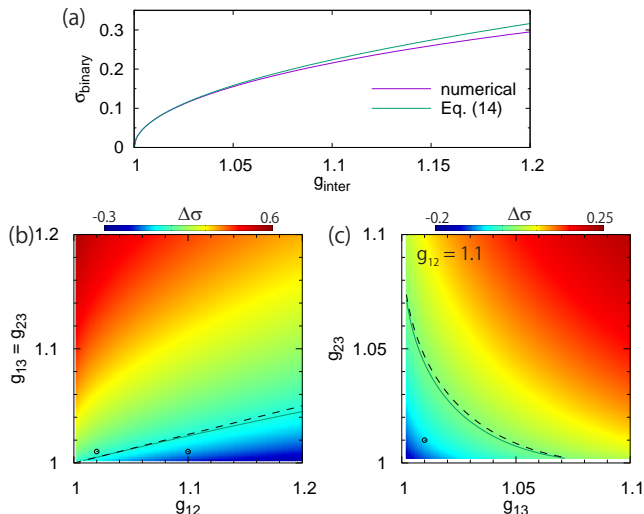


FIG. 4. (a) Interfacial tension σ_{binary} for a two-component BEC as a function of the intercomponent interaction g_{inter} . The numerical result is compared with Eq. (14). (b) and (c) Dependence of $\Delta\sigma$ in Eq. (15) on the intercomponent interactions g_{12} , g_{23} , and g_{13} , where the values of σ_{binary} in Eq. (15) are taken from the numerical result in (a). In (c), g_{12} is fixed to 1.1. The solid lines represent the contour of $\Delta\sigma = 0$, and the dashed lines are Eq. (16). The points correspond to the parameters used in Fig. 3(a).

values agree well with the approximation in Eq. (14): $\sqrt{(1.1-1)/2} \simeq 0.224$ and $\sqrt{(1.02-1)/2} \simeq 0.1$. In Fig. 3(a), the interfacial tension converges to $\sigma \simeq 0.141$ for large n_3 . This value of the interfacial tension should be $\sigma_{\text{binary}}(g_{13}) + \sigma_{\text{binary}}(g_{23}) = 2\sigma_{\text{binary}}(1.01)$, since the three-component interface consists of two separate interfaces (1-3 and 2-3 interfaces) for large n_3 , as shown in the bottom panel in Fig. 2(a). Using Eq. (14) with $g_{13} = g_{23} = 1.01$, we get $\sigma_{\text{binary}}(g_{13}) + \sigma_{\text{binary}}(g_{23}) \simeq 2\sqrt{(1.01-1)/2} \simeq 0.141$, which is in good agreement with the value obtained above.

The surfactant behavior of component 3 is understood as follows. When component 3 is absent, i.e., when components 1 and 2 are in direct contact, the interfacial tension $\sigma = \sigma_{\text{inter}}(g_{12})$ is large, since g_{12} is large. This is because the one component cannot penetrate into the other for large g_{12} , and the densities have to change abruptly at the interface, which results in a large interfacial tension according to Eq. (11). When component 3 is inserted into the interface, component 3 mediates between components 1 and 2. Since g_{13} and g_{23} are not so large, the density variation in each component is moderate across this 1-3-2 interface. In fact, the slopes of $|\psi_1|^2$ and $|\psi_2|^2$ at the interface in Fig. 2(a) for $n_3 \geq 10$ are more gradual than those for $n_3 = 0$. Thus, the interfacial tension is decreased by component 3.

As shown in Fig. 2(a), $\sigma = \sigma_{\text{binary}}(g_{12})$ for $n_3 = 0$ and σ converges to $\sigma_{\text{binary}}(g_{13}) + \sigma_{\text{binary}}(g_{23})$ for large

n_3 . Therefore, their difference,

$$\Delta\sigma \equiv \sigma_{\text{binary}}(g_{13}) + \sigma_{\text{binary}}(g_{23}) - \sigma_{\text{binary}}(g_{12}), \quad (15)$$

characterizes the surfactant behavior of the system; component 3 serves as a surfactant when $\Delta\sigma < 0$. Equation (15) only includes the interfacial tension of a two-component BEC. We numerically obtain $\sigma_{\text{binary}}(g_{\text{inter}})$ as a function of g_{inter} using the two-component version of Eqs. (11) and (12), which is shown in Fig. 4(a). The numerical result agrees well with the approximate expression in Eq. (14) for g_{inter} close to unity. Using the numerically obtained $\sigma_{\text{binary}}(g_{\text{inter}})$, we calculate $\Delta\sigma$ in Eq. (15), which is plotted in Figs. 4(b) and 4(c). The solid lines in Figs. 4(b) and 4(c) represent the contours of $\Delta\sigma = 0$, and the surfactant regions of $\Delta\sigma < 0$ lie below these lines. Using the approximate expression in Eq. (14), $\Delta\sigma = 0$ reads

$$\sqrt{g_{13}-1} + \sqrt{g_{23}-1} - \sqrt{g_{12}-1} = 0, \quad (16)$$

which is represented by the dashed lines in Figs. 4(b) and 4(c). These are in good agreement with the solid lines.

B. Variational analysis

We perform variational analysis for better understanding of the numerical results in Sec. II A. We use the following form of the variational wave functions:

$$\psi_1^{(\text{var})}(z) = \sqrt{\frac{1}{2}} \left(1 - \tanh \frac{z+z_0}{\alpha} \right), \quad (17a)$$

$$\psi_2^{(\text{var})}(z) = \sqrt{\frac{1}{2}} \left(1 + \tanh \frac{z-z_0}{\alpha} \right), \quad (17b)$$

$$\psi_3^{(\text{var})}(z) = \sqrt{\frac{1}{2}} \left(\tanh \frac{z+w/2}{\alpha} - \tanh \frac{z-w/2}{\alpha} \right), \quad (17c)$$

where z_0 and α are variational parameters characterizing the position and width of the interface. At infinity $z \rightarrow \pm\infty$, these variational functions have the same limiting behaviors as the wave functions in Sec. II A, i.e., $\psi_1^{(\text{var})} \rightarrow 1$ and $\psi_2^{(\text{var})} \rightarrow 0$ for $z \rightarrow -\infty$, and $\psi_1^{(\text{var})} \rightarrow 0$ and $\psi_2^{(\text{var})} \rightarrow 1$ for $z \rightarrow \infty$. In Eq. (17c), the parameter w determines the number of atoms in component 3, because

$$\int_{-\infty}^{\infty} dz |\psi_3^{(\text{var})}(z)|^2 = w. \quad (18)$$

If $z_0 = w$, Eq. (17) gives the uniform total density, $|\psi_1^{(\text{var})}(z)|^2 + |\psi_2^{(\text{var})}(z)|^2 + |\psi_3^{(\text{var})}(z)|^2 = 1$. Substituting the variational wave functions in Eq. (17) into the grand potential in Eq. (2), and subtracting the divergent part, we obtain the variational grand potential Ω_{var} (see

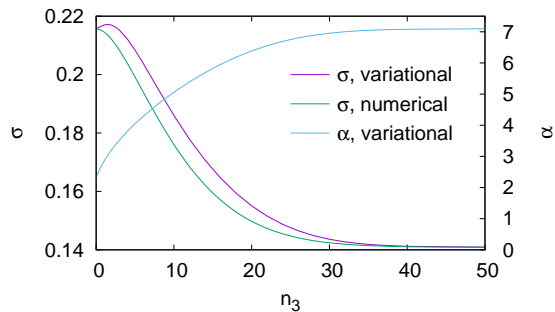


FIG. 5. Comparison between the interfacial tension σ obtained by the variational method (“ σ , variational”) and that obtained by solving the GP equation (“ σ , numerical”, the same data as in Fig. 3(a)) for $g_{12} = 1.1$ and $g_{13} = g_{23} = 1.01$. The variational parameter α minimizing the variational energy is also shown (“ α , variational”).

Appendix A for derivation). We minimize Ω_{var} with respect to z_0 and α . Using these optimal values of z_0 and α , we calculate the interfacial tension via

$$\begin{aligned} \sigma &= 2 \int_{-\infty}^{\infty} dz \sum_{j=1}^3 \frac{1}{2} \left(\frac{d\psi_j^{(\text{var})}}{dz} \right)^2 \\ &= \frac{1}{2\alpha} + \frac{1}{2\alpha^2} \left[\alpha \coth \frac{w}{\alpha} - w \left(\sinh \frac{w}{\alpha} \right)^{-2} \right]. \end{aligned} \quad (19)$$

Figure 5 compares the interfacial tension obtained by the variational method with that obtained in Fig. 3(a) numerically. The variationally obtained σ agrees well with the numerically obtained σ for $n_3 = 0$ and $n_3 \gtrsim 40$. In the intermediate region of n_3 , the former deviates slightly from the latter, which is due to the simple form of the variational wave function in Eq. (17). The optimal variational parameter α that corresponds to the interface width is also shown in Fig. 5. The value of α increases with n_3 , and therefore, our variational wave function captures the basic physics of the surfactant behavior: the spatial variation in the densities at the interface is made gradual by component 3.

C. Thermodynamic relations

According to the definition of interfacial tension σ , the work required for increasing the interface area A by dA is given by σdA . Thus, at zero temperature and in a fixed volume, the energy differential is given by $dE = \sum_j \mu_j dN_j + \sigma dA$, and therefore the differential of the grand potential has the form,

$$d\Omega = - \sum_{j=1}^3 N_j d\mu_j + \sigma dA. \quad (20)$$

This differential relation leads to

$$\frac{\partial \Omega}{\partial \mu_j} = -N_j. \quad (21)$$

In general, the grand potential Ω can be divided into a volume part and an interface part σA , as shown in Eq. (10) for a flat interface, where the interface part corresponds to the second term on the right-hand side of Eq. (10). Since component 3 is localized at the interface, μ_3 is included only in the interface part σA of the grand potential, and therefore,

$$\frac{\partial \Omega}{\partial \mu_3} = A \frac{\partial \sigma}{\partial \mu_3}. \quad (22)$$

From Eqs. (21) and (22), we obtain

$$\frac{\partial \sigma}{\partial \mu_3} = -\frac{N_3}{A}. \quad (23)$$

We have numerically confirmed that this relation holds for Fig. 2(b), i.e., $d\sigma/d\mu_3 = n_3$.

We assume that the volume part of the system is sufficiently large, and $N_1, N_2 \rightarrow \infty$ with μ_1 and μ_2 being fixed. In this case, σ is a function of only μ_3 or N_3 , as in the case of Fig. 2. It follows from Eq. (23) that

$$\frac{d\sigma}{dN_3} = -\frac{N_3}{A} \frac{d\mu_3}{dN_3}. \quad (24)$$

Integrating this equation with respect to N_3 , we have

$$\sigma = -\frac{1}{A} \int N_3 \frac{d\mu_3}{dN_3} dN_3 + c, \quad (25)$$

where we determine the integration constant c appropriately. When $N_3 = 0$, σ should be the two-component interfacial tension $\sigma_{\text{binary}}(g_{12})$, and hence,

$$\sigma = -\frac{1}{A} \int_0^{N_3} N_3 \frac{d\mu_3}{dN_3} dN_3 + \sigma_{\text{binary}}(g_{12}). \quad (26)$$

In the limit of $N_3 \rightarrow \infty$, the interfacial tension should approach $\sigma \rightarrow \sigma_{\text{binary}}(g_{13}) + \sigma_{\text{binary}}(g_{23})$, giving

$$\sigma = \frac{1}{A} \int_{N_3}^{\infty} N_3 \frac{d\mu_3}{dN_3} dN_3 + \sigma_{\text{binary}}(g_{13}) + \sigma_{\text{binary}}(g_{23}). \quad (27)$$

Using Eqs. (26) and (27), $\Delta\sigma$ defined in Eq. (15) can be written as

$$\Delta\sigma = -\frac{1}{A} \int_0^{\infty} N_3 \frac{d\mu_3}{dN_3} dN_3. \quad (28)$$

A similar relation is derived for the wetting problem in Ref. [41]. Interestingly, $\Delta\sigma$ in Eq. (28) is expressed in terms of only μ_3 and N_3 . We have numerically confirmed that the relation (28) is satisfied for the flat interface in Sec. II A.

D. Bogoliubov analysis

We perform Bogoliubov analysis to study the dynamical stability of the flat interface discussed in Sec. II A. We

consider a small deviation $\delta\psi_j(\mathbf{r}, t)$ from the stationary state $f_j(z)$ with a flat interface located around the $z = 0$ plane, and therefore, the wave function can be broken down into

$$\psi_j(\mathbf{r}, t) = e^{-i\mu_j t/\hbar} [f_j(z) + \delta\psi_j(\mathbf{r}, t)], \quad (29)$$

where $f_j(z)$ is the solution for Eq. (7) obtained by the imaginary-time evolution of Eq. (12). Substitution of Eq. (29) into the time-dependent GP equation,

$$i\frac{\partial\psi_j}{\partial t} = -\frac{1}{2}\nabla^2\psi_j + \sum_{j'=1}^3 g_{jj'} |\psi_{j'}|^2 \psi_j, \quad (30)$$

gives

$$i\frac{\partial\delta\psi_j}{\partial t} = -\frac{1}{2}\nabla^2\delta\psi_j - \mu_j\delta\psi_j + \sum_{j'=1}^3 g_{jj'} (|f_{j'}|^2\delta\psi_j + f_{j'}^* f_j \delta\psi_{j'} + f_{j'} f_j \delta\psi_{j'}^*). \quad (31)$$

The small deviation $\delta\psi_j(\mathbf{r}, t)$ can be decomposed into Fourier components, and we focus on a plane wave with wave number \mathbf{k}_\perp along the interface:

$$\delta\psi_j(\mathbf{r}, t) = u_j(z)e^{i\mathbf{k}_\perp \cdot \mathbf{r}_\perp - i\omega t} + v_j^*(z)e^{-i\mathbf{k}_\perp \cdot \mathbf{r}_\perp + i\omega^* t}, \quad (32)$$

where the subscript \perp indicates that the vector is in the x - y plane. Substituting Eq. (32) into Eq. (31), we obtain the following Bogoliubov-de Gennes equations:

$$\omega u_j = -\frac{1}{2}u_j'' + \left(\frac{k_\perp^2}{2} - \mu_j\right)u_j + \sum_{j'=1}^3 g_{jj'} (|f_{j'}|^2 u_j + f_{j'} f_{j'}^* u_{j'} + f_j f_{j'} v_{j'}), \quad (33a)$$

$$-\omega v_j = -\frac{1}{2}v_j'' + \left(\frac{k_\perp^2}{2} - \mu_j\right)v_j + \sum_{j'=1}^3 g_{jj'} (|f_{j'}|^2 v_j + f_j f_{j'}^* v_{j'} + f_j f_{j'} u_{j'}), \quad (33b)$$

which are six simultaneous differential equations.

We spatially discretize $u_j(z)$ and $v_j(z)$ in Eq. (33) and approximate the second derivative by $u_j'' \simeq [u_j(z + \delta z) - 2u_j(z) + u_j(z - \delta z)]/\delta z^2$, which gives the matrix form of the eigenvalue equation. We numerically diagonalize the eigenvalue equation to obtain the eigenfrequency ω . If ω is real for any k_\perp , the stationary flat interface state is dynamically stable. If the imaginary part of ω is nonzero, the corresponding mode grows in time exponentially, and the system is dynamically unstable.

Figure 6 shows the lowest excitation frequency ω_L that has the smallest real part among the frequencies ω . For the parameters investigated in Fig. 6, only ω_L becomes complex and other ω are found to be real. In Fig. 6(a), we first examine the interaction parameters used in Fig. 3(a) with $n_3 = 10$ being fixed. For $g_{12} = 1.1$, which corresponds to the surfactant behavior in Fig. 3(a), $\text{Re}\omega_L$ increases with k_\perp while $\text{Im}\omega_L = 0$, and the flat interface is dynamically stable. We confirmed that this stability

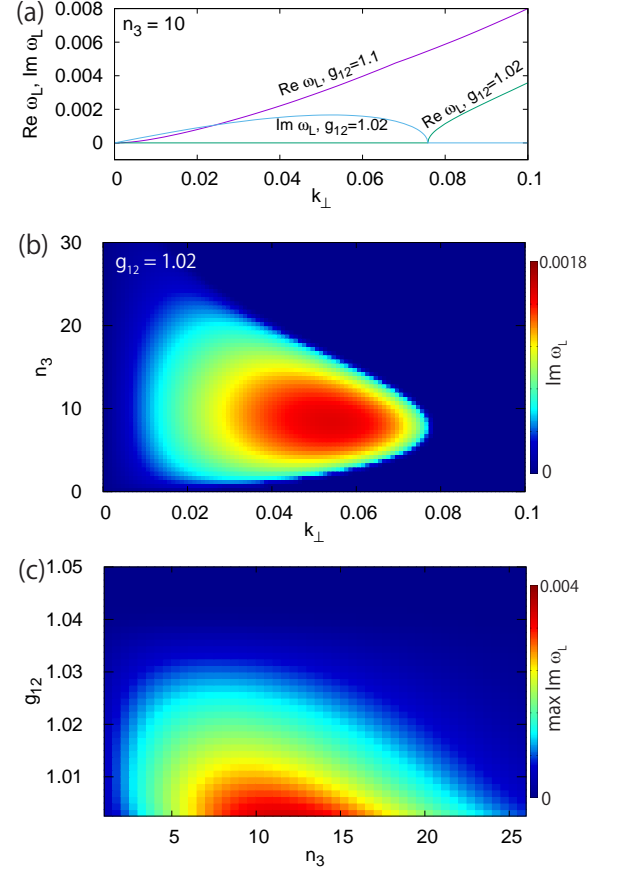


FIG. 6. Lowest excitation frequency ω_L obtained by numerically diagonalizing Eq. (33). (a) Real and imaginary parts of ω_L as functions of k_\perp for $g_{12} = 1.1$, $g_{12} = 1.02$, and $n_3 = 10$. For $g_{12} = 1.1$, $\text{Im}\omega = 0$ for all the excitations. (b) Imaginary part of ω_L as a function of k_\perp and n_3 for $g_{12} = 1.02$. (c) Largest imaginary part $\max \text{Im}\omega_L$ with respect to k_\perp as a function of n_3 and g_{12} . In (a)-(c), g_{13} and g_{23} are fixed to 1.01.

is maintained for any n_3 , and the interface with surfactant behavior considered in Fig. 3(a) is always stable. For $g_{12} = 1.02$, on the other hand, ω_L is purely imaginary for $0 < k_\perp \lesssim 0.076$. The imaginary part $\text{Im}\omega_L$ is the largest for $k_\perp \simeq 0.05$, and the interface is the most unstable in this wavelength.

Figure 6(b) shows $\text{Im}\omega_L$ as a function of k_\perp and n_3 for $g_{12} = 1.02$, and Fig. 6(c) shows the largest imaginary part $\max \text{Im}\omega_L(k_\perp)$ among all k_\perp as a function of n_3 and g_{12} . Figures 6(b) and 6(c) show that the interface stabilizes for $n_3 = 0$ and $n_3 \gtrsim 30$. This is deduced from the fact that an isolated two-component interface is always stable; for $n_3 = 0$, the interface reduces to the 1-2 interface, and for large n_3 , the 1-3 and 2-3 interfaces separate and can be regarded two distinct two-component interfaces. It follows from this result that instability arises from the interaction among the three components, including the interaction between components 1 and 2 across the

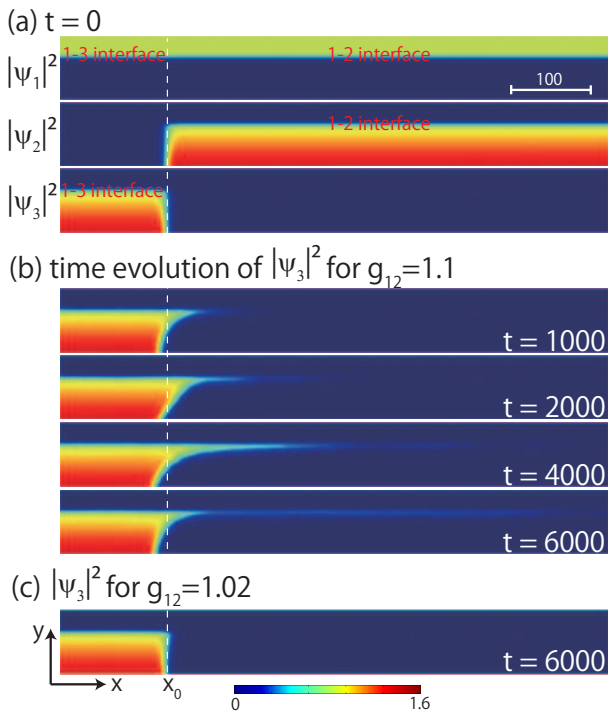


FIG. 7. Dynamics of interface flow due to a gradient in interfacial tension: Marangoni flow. (a) Initial density distribution of the three components, which is the ground state for $g_{12} = g_{13} = g_{23} = 1.01$. (b) Time evolution after g_{12} is changed from 1.01 to 1.1 at $t = 0$. (c) Snapshot at $t = 6000$, where g_{12} is changed from 1.01 to 1.02 at $t = 0$. The vertical dashed line indicates the initial position of the 2-3 interface x_0 . See supplemental material for videos of the dynamics in (b) and (c) [44].

layer of component 3. After dynamical instability sets in, droplets of component 3 are formed, as seen in capillary instability [28].

III. DYNAMIC PROPERTIES: MARANGONI FLOW

When there is a spatial gradient in the interfacial tension σ along the interface, the interface with larger σ pulls the interface with smaller σ , which results in a flow along the interface. Such an interface flow driven by the interfacial tension gradient is referred to as a Marangoni flow [42]. The Marangoni effect can be observed in daily life: for example, tears of wine [43] and stabilization of soap films. The Marangoni effect is also important in the formation of Bénard cells in convection. In these examples, the gradient in the surface or interfacial tension is caused by the gradients in solute concentration and in temperature.

Here we numerically demonstrate the Marangoni-like flow in the three-component BEC in a two-dimensional system. To realize the interfacial tension gradient along the interface, we consider the situation shown in

Fig. 7(a). The 1-2 and 1-3 interfaces are straight along the x direction, and components 2 and 3 are located in the regions of $x \gtrsim x_0$ and $x \lesssim x_0$, respectively, where x_0 is the position of the 2-3 interface. The interaction coefficients are initially taken to be $g_{12} = g_{13}$, and the interfacial tensions of the 1-2 and 1-3 interfaces are the same in the initial state. At $t = 0$, we suddenly increase g_{12} , which increases the interfacial tension of the 1-2 interface. Consequently, the horizontal interface acquires a gradient along the x direction, i.e., the interfacial tension at $x \gtrsim x_0$ exceeds that at $x \lesssim x_0$, and we presume that the 1-2 interface entrains the 1-3 interface in the $+x$ direction.

We perform a numerical simulation of the time-dependent GP equation:

$$i \frac{\partial \psi_j}{\partial t} = -\frac{1}{2} \nabla^2 \psi_j + V_j \psi_j + \sum_{j'=1}^3 g_{jj'} |\psi_{j'}|^2 \psi_j. \quad (34)$$

The initial state is the ground state for $g_{12} = g_{13} = g_{23} = 1.01$, as shown in Fig. 7(a), which is obtained by the imaginary-time evolution of Eq. (34). The number of atoms N_j in each component is chosen such that the density becomes $|\psi_j|^2 \simeq 1$ near the horizontal interface. At $t = 0$, g_{12} is increased abruptly, and the real-time evolution is calculated. To maintain a straight interface through the imaginary- and real-time evolutions, we apply a potential $V_2 = V_3 = 0.01y$ ($V_1 = 0$), which exerts a weak force on components 2 and 3 in the $-y$ direction. Because the size of the whole system is sufficiently large, the boundary does not affect the dynamics shown.

Figure 7(b) shows the time evolution of the density distribution of component 3, where g_{12} is changed from 1.01 to 1.1 at $t = 0$. As a result of this change, the interfacial tension at the 1-2 interface becomes $\sigma = \sigma_{\text{binary}}(1.1) \simeq 0.216$, while $\sigma = \sigma_{\text{binary}}(1.01) \simeq 0.071$ at the 1-3 interface. As expected, the 1-2 interface pulls the 1-3 interface into the $+x$ direction, and component 3 flows into the $+x$ direction near the interface. This interface flow leads to a three-component (1-3-2) interface in the region $x > x_0$. The interfacial tension of this 1-3-2 interface is still smaller than that of the 1-2 interface, according to Fig. 3(a) (the line $g_{12} = 1.1$), and therefore, component 3 flows further into the $x > x_0$ region as time elapses. Figure 7(c) shows the case where g_{12} is changed from 1.01 to 1.02 at $t = 0$. In this case, no Marangoni-like flow is observed, even though there is a gradient in interfacial tension. This is because, for $g_{12} = 1.02$, the interfacial tension increases with n_3 , as shown in Fig. 3(a); even if the 1-3-2 interface were formed, its interfacial tension would be larger than that of the 1-2 interface, and the 1-3-2 interface would be pulled back in the $-x$ direction. Thus, the flow of component 3 into the 1-2 interface is suppressed.

IV. CONCLUSIONS

We have investigated the static and dynamic properties of an interface in an immiscible three-component BEC. We considered the case illustrated in Fig. 1, where component 3 was sandwiched by components 1 and 2. We calculated the interfacial tension of the three-component interface and showed that a component 3 inserted into the 1-2 interface can lower the interfacial tension, i.e., it can play the role of surfactant (Fig. 3). We obtained the dependence of the interfacial tension on various parameters (Figs. 3 and 4). We proposed a variational wave function for understanding the surfactant behavior qualitatively (Sec. II B). The stability of the three-component interface was examined by Bogoliubov analysis (Fig. 6), and it was shown that the three-component interface is dynamically stable when component 3 plays the role of surfactant. Finally, we studied the case shown in Fig. 7 to demonstrate that an interfacial tension gradient induces a Marangoni-like flow. We showed that an interface with smaller interfacial tension is entrained toward an interface with larger interfacial tension, resulting in interfacial flow.

An extension of this study would be to focus on emulsification in turbulent superfluids. When oil and water are stirred, the large interfacial tension between oil and water prevents their droplets from becoming small. By adding a surfactant, the interfacial tension between oil and water decreases, allowing the droplets to become smaller, i.e., emulsified. We would expect to see a similar trend in a stirred three-component BEC upon the addition of the third component. This phenomenon may be realized given the recent developments in quantum-turbulence experiments in BECs [45, 46].

ACKNOWLEDGMENTS

This work was supported by JSPS KAKENHI Grant Number JP20K03804.

Appendix A: Calculation of the variational grand potential

We calculate the grand potential in Eq. (2) using the variational wave function in Eq. (17). Substituting Eq. (17) into the kinetic energy,

$$E_j^{(\text{kin})} = -\frac{1}{2} \int_{-\infty}^{\infty} dz \psi_j^{(\text{var})*} \frac{d^2 \psi_j^{(\text{var})}}{dz^2}, \quad (\text{A1})$$

we obtain

$$E_1^{(\text{kin})} = E_2^{(\text{kin})} = \frac{1}{8\alpha} \quad (\text{A2})$$

and

$$E_3^{(\text{kin})} = \frac{1}{4\alpha^2} \left[\alpha \coth \frac{w}{\alpha} - w \left(\sinh \frac{w}{\alpha} \right)^{-2} \right]. \quad (\text{A3})$$

Since we are considering an infinite space, the intracomponent interaction and the chemical potential part,

$$E_j^{(\text{intra})} = \int_{-\infty}^{\infty} dz \left(\frac{g_{jj}}{2} |\psi_j^{(\text{var})}|^4 - \mu_j |\psi_j^{(\text{var})}|^2 \right), \quad (\text{A4})$$

diverge for $j = 1$ and 2 , and we must subtract the divergent part from them. For $j = 1$, the indefinite integral of Eq. (A4) is calculated to be (we are assuming $g_{11} = 1$ and $\mu_1 = 1$)

$$\begin{aligned} & \int dz \left(\frac{1}{2} |\psi_j^{(\text{var})}|^4 - |\psi_j^{(\text{var})}|^2 \right) \\ &= -\frac{z}{4} + \frac{\alpha}{4} \ln \cosh \frac{z+z_0}{\alpha} - \frac{\alpha}{8} \tanh \frac{z+z_0}{\alpha}, \end{aligned} \quad (\text{A5})$$

which approaches

$$-\frac{z}{2} + \frac{1}{8} [\alpha(1 - \ln 4) - 2z_0] \quad (z \rightarrow -\infty), \quad (\text{A6a})$$

$$\frac{1}{8} [\alpha(-1 - \ln 4) + 2z_0] \quad (z \rightarrow \infty). \quad (\text{A6b})$$

The divergence stems from the term $-z/2$ in Eq. (A6a). Since this divergent part does not include the variational parameters, we can drop this term in the variational analysis. Thus, the regularized form of the definite integral in Eq. (A4) becomes

$$E_1^{(\text{intra})} = \frac{1}{4} (2z_0 - \alpha). \quad (\text{A7})$$

Since $\psi_2^{(\text{var})}(z) = \psi_1^{(\text{var})}(-z)$, we have the same result for $j = 2$: $E_2^{(\text{intra})} = (2z_0 - \alpha)/4$. For $j = 3$, there is no divergence, and we obtain

$$E_3^{(\text{intra})} = \frac{1}{2} \left(w \coth \frac{w}{\alpha} - \alpha \right) - \mu_3 w. \quad (\text{A8})$$

The integrals $I_{jj'} \equiv \int_{-\infty}^{\infty} dz |\psi_j^{(\text{var})}|^2 |\psi_{j'}^{(\text{var})}|^2$ in the inter-component interaction energies are calculated to be

$$I_{12} = \frac{2z_0}{e^{4z_0/\alpha} - 1}, \quad (\text{A9})$$

and

$$I_{13} = I_{23} = \frac{1}{2} \left(\frac{w - 2x_0}{1 - e^{(2z_0 - w)/\alpha}} + \frac{w + 2x_0}{1 - e^{(2z_0 + w)/\alpha}} \right). \quad (\text{A10})$$

The variational grand potential Ω_{var} is thus obtained from Eqs. (A2), (A3), (A7), (A8), (A9), and (A10):

$$\Omega_{\text{var}} = \sum_{j=1}^3 \left(E_j^{(\text{kin})} + E_j^{(\text{intra})} \right) + g_{12} I_{12} + g_{13} I_{13} + g_{23} I_{23}. \quad (\text{A11})$$

-
- [1] C. J. Myatt, E. A. Burt, R. W. Ghrist, E. A. Cornell, and C. E. Wieman, *Phys. Rev. Lett.* **78**, 586 (1997).
- [2] G. Modugno, M. Modugno, F. Riboli, G. Roati, and M. Inguscio, *Phys. Rev. Lett.* **89**, 190404 (2002).
- [3] S. B. Papp, J. M. Pino, and C. E. Wieman, *Phys. Rev. Lett.* **101**, 040402 (2008).
- [4] S. Tojo, Y. Taguchi, Y. Masuyama, T. Hayashi, H. Saito, and T. Hirano, *Phys. Rev. A* **82**, 033609 (2010).
- [5] D. S. Hall, M. R. Matthews, J. R. Ensher, C. E. Wieman, and E. A. Cornell, *Phys. Rev. Lett.* **81**, 1539 (1998).
- [6] H.-J. Miesner, D. M. Stamper-Kurn, J. Stenger, S. Inouye, A. P. Chikkatur, and W. Ketterle, *Phys. Rev. Lett.* **82**, 2228 (1999).
- [7] K. M. Mertes, J. W. Merrill, R. Carretero-González, D. J. Frantzeskakis, P. G. Kevrekidis, and D. S. Hall, *Phys. Rev. Lett.* **99**, 190402 (2007).
- [8] Y. Eto, M. Kunimi, H. Tokita, H. Saito, and T. Hirano, *Phys. Rev. A* **92**, 013611 (2015).
- [9] T.-L. Ho and V. B. Shenoy, *Phys. Rev. Lett.* **77**, 3276 (1996).
- [10] H. Pu and N. P. Bigelow, *Phys. Rev. Lett.* **80**, 1130 (1998).
- [11] E. Timmermans, *Phys. Rev. Lett.* **81**, 5718 (1998).
- [12] P. Ao and S. T. Chui, *Phys. Rev. A* **58**, 4836 (1998).
- [13] M. Trippenbach, K. Góral, K. Rzazewski, B. Malomed, Y. B. Band, *J. Phys. B* **33**, 4017 (2000).
- [14] I. E. Mazets, *Phys. Rev. A* **65**, 033618 (2002).
- [15] R. A. Barankov, *Phys. Rev. A* **66**, 013612 (2002).
- [16] B. Van Schaeybroeck, *Phys. Rev. A* **78**, 023624 (2008); *Phys. Rev. A* **80**, 065601 (2009).
- [17] H. Takeuchi and K. Kasamatsu, *Phys. Rev. A* **88**, 043612 (2013).
- [18] J. O. Indekeu, C.-Y. Lin, N. Van Thu, B. Van Schaeybroeck, and T. H. Phat, *Phys. Rev. A* **91**, 033615 (2015).
- [19] K. L. Lee, N. B. Jørgensen, I.-K. Liu, L. Wacker, J. J. Arlt, and N. P. Proukakis, *Phys. Rev. A* **94**, 013602 (2016).
- [20] N. V. Thu, T. H. Phat, and P. T. Song, *J. Low Temp. Phys.* **186**, 127 (2017).
- [21] J. O. Indekeu, N. Van Thu, C.-Y. Lin, and T. H. Phat, *Phys. Rev. A* **97**, 043605 (2018).
- [22] K. Sasaki, N. Suzuki, D. Akamatsu, and H. Saito, *Phys. Rev. A* **80**, 063611 (2009).
- [23] S. Gautam and D. Angom, *Phys. Rev. A* **81**, 053616 (2010).
- [24] H. Takeuchi, N. Suzuki, K. Kasamatsu, H. Saito, and M. Tsubota, *Phys. Rev. B* **81**, 094517 (2010).
- [25] A. Bezett, V. Bychkov, E. Lundh, D. Kobayakov, and M. Marklund, *Phys. Rev. A* **82**, 043608 (2010).
- [26] N. Suzuki, H. Takeuchi, K. Kasamatsu, M. Tsubota, and H. Saito, *Phys. Rev. A* **82**, 063604 (2010).
- [27] D. Kobayakov, V. Bychkov, E. Lundh, A. Bezett, V. Akkerman, and M. Marklund, *Phys. Rev. A* **83**, 043623 (2011).
- [28] K. Sasaki, N. Suzuki, and H. Saito, *Phys. Rev. A* **83**, 053606 (2011).
- [29] T. Kadokura, T. Aioi, K. Sasaki, T. Kishimoto, and H. Saito, *Phys. Rev. A* **85**, 013602 (2012).
- [30] D. Kobayakov, A. Bezett, E. Lundh, M. Marklund, and V. Bychkov, *Phys. Rev. A* **85**, 013630 (2012).
- [31] D. Kobayakov, V. Bychkov, E. Lundh, A. Bezett, and M. Marklund, *Phys. Rev. A* **86**, 023614 (2012).
- [32] H. Sakaguchi and H. Chono, *Phys. Rev. E* **96**, 052222 (2017).
- [33] D. K. Maity, K. Mukherjee, S. I. Mistakidis, S. Das, P. G. Kevrekidis, S. Majumder, and P. Schmelcher, *Phys. Rev. A* **102**, 033320 (2020).
- [34] We are not including spinor BECs in this discussion. For the interfaces of spinor BECs, see for example, Refs. [35–37].
- [35] M. O. Borgh and J. Ruostekoski, *Phys. Rev. Lett.* **109**, 015302 (2012).
- [36] M. O. Borgh and J. Ruostekoski, *Phys. Rev. A* **87**, 033617 (2013).
- [37] T. Kaneda and H. Saito, *Phys. Rev. A* **90**, 053632 (2014).
- [38] See, e.g., C. J. Pethick and H. Smith, *Bose-Einstein condensation in dilute gases*, 2nd ed., Chap. 12. (Cambridge Univ. Press, Cambridge, 2008).
- [39] D. C. Roberts and M. Ueda, *Phys. Rev. A* **73**, 053611 (2006).
- [40] W. H. Press, S. A. Teukolsky, W. T. Vetterling, and B. P. Flannery, *Numerical Recipes*, 3rd ed. (Cambridge Univ. Press, Cambridge, 2007).
- [41] L. D. Landau and E. M. Lifshitz, *Statistical Physics*, 3rd ed. part 1 (Butterworth-Heinemann, Oxford, 1980), Chap. XV.
- [42] L. E. Scriven and C. V. Sternling, *Nature* **187**, 186 (1960).
- [43] J. Thomson, *Phil. Mag.* **10**, 330 (1855).
- [44] See Supplemental Material at <http://link.aps.org/supplemental/...> for videos of the dynamics.
- [45] N. Navon, A. L. Gaunt, R. P. Smith, and Z. Hadzibabic, *Nature (London)* **539**, 72 (2016).
- [46] N. Navon, C. Eigen, J. Zhang, R. Lopes, A. L. Gaunt, K. Fujimoto, M. Tsubota, R. P. Smith, and Z. Hadzibabic, *Science* **366**, 382 (2019).